Journal of Power Sources 219 (2012) 364–370

Contents lists available at SciVerse ScienceDirect

Journal of Power Sources

journal homepage: www.elsevier.com/locate/jpowsour

Short communication

3-dimensional carbon nanotube for Li-ion battery anode

Chiwon Kang [a,1], Indranil Lahiri [a,1], Rangasamy Baskaran [b], Won-Gi Kim [b], Yang-Kook Sun [b], Wonbong Choi [a,b,c,*]

[a] Nanomaterials and Device Laboratory, Department of Mechanical and Materials Engineering, Florida International University, 10555 West Flagler Street, Miami, FL 33174, USA
[b] Department of Energy Engineering, Hanyang University, 17 Haengdang-dong, Seongdong-gu, Seoul 133-791, South Korea
[c] Department of Materials Science and Engineering, University of North Texas, North Texas Discovery Park 3940 North Elm St. Suite E-132, Denton, TX 76207, USA

HIGHLIGHTS

- A novel 3-dimensional design of anode improves surface area utilization factor.
- High surface area of 3D Cu leads to higher MWCNT loading and better performance.
- Amorphous Si coating further enhances the performance of the 3D MWCNT-based anode.

GRAPHICAL ABSTRACT

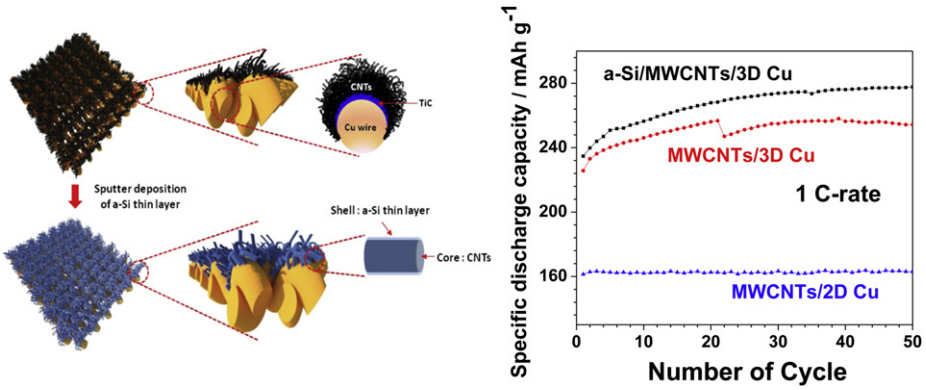

ARTICLE INFO

Article history:
Received 11 May 2012
Received in revised form
14 July 2012
Accepted 16 July 2012
Available online 24 July 2012

Keywords:
Li-ion batteries
Carbon nanotubes
3D Cu current collector
Anode materials
Amorphous Si
a-Si/MWCNTs composite

ABSTRACT

Carbon nanotubes, in different forms and architectures, have demonstrated good promise as electrode material for Li-ion batteries, owing to large surface area, shorter Li-conduction distance and high electrical conductivity. However, practical application of such Li-ion batteries demands higher volumetric capacity, which is otherwise low for most nanomaterials, used as electrodes. In order to address this urgent issue, we have developed a novel 3-dimensional (3D) anode, based on multiwall carbon nanotubes (MWCNTs), for Li-ion batteries. The unique 3D design of the electrode allowed much higher solid loading of active anode material, MWCNTs in this case and resulted in more amount of Li^+ ion intake in comparison to those of conventional 2D Cu current collector. Though one such 3D anode was demonstrated to offer 50% higher capacity, compared to its 2D counterpart, its ability to deliver much higher capacity, by geometrical modification, is presented. Furthermore, deposition of amorphous Si (a-Si) layer on the 3D electrode (a-Si/MWCNTs hybrid structure) offered enhancement in electrochemical response. Correlation between electrochemical performances and structural properties of the 3D anodes highlights the possible charge transfer mechanism.

1. Introduction

Li-ion battery (LIB) has been widely used as one of the most important energy storage devices in diverse applications such as green electric vehicles (EV), portable electronics and power tools, since it is commercialized by Sony in 1991 [1]. The commercial cell

* Corresponding author. Nanomaterials and Device Laboratory, Department of Mechanical and Materials Engineering, Florida International University, 10555 West Flagler Street, Miami, FL 33174, USA. Tel.: +1 305 348 1973; fax: +1 305 348 1932.
E-mail address: choiw@fiu.edu (W. Choi).
[1] These authors contributed equally.

0378-7753/$ – see front matter © 2012 Published by Elsevier B.V.
http://dx.doi.org/10.1016/j.jpowsour.2012.07.050

is assembled by carbonaceous anode, separator and a Li containing layered structure cathode (e.g. $LiCoO_2$). In terms of carbonaceous anodes, graphite and soft or poorly ordered carbons (e.g. mesocarbon microbeads or spherical graphite, microcarbon fiber) have been employed. The reasons behind their commercial prominence contain the relatively low cost of carbon, the excellent mechanical sustainability for lithium insertion and desertion (having minimum volume change) and their formation of a protective surface film with many electrolytes [2–4]. Nevertheless, fully intercalated highly crystalline graphites have relatively lower specific capacity (372 $mAhg^{-1}$, the stoichiometric formulae of LiC_6) and cannot meet the demands of next generation LIB with respect to high specific capacity and volumetric capacity. To address these issues, other elemental compounds have been explored such as Al, Si, Ge and Sn [5]. Among those elements, Si is known to have highest theoretical specific capacity (4200 $mAhg^{-1}$), however huge volume expansion/contraction (300–400%) during lithiation/delithiation brings about pulverization, resulting in capacity fading in a high number of cycles. To overcome such inherit limitations of bulk electrode materials, worldwide research groups have intensively focused on novel and suitable nanomaterials such as silicon nanotubes [6], silicon nanowires [7], nanosized transitional metal oxides [8–10], graphene [11] and carbon nanotubes [12–14].

Out of the many available nanomaterials, carbon nanotubes (CNTs) have attracted great attention for anode materials due to their high surface area, short diffusion length of Li^+ ions and high electrical conductivity [15]. Past researches including from our group have demonstrated outstanding performance of MWCNT-based binder-free anodes in terms of high specific capacity, excellent rate capability and almost no capacity degradation during long cycle operation [16,17]. However, carbon nanomaterials are known as low-density materials, which results in low volumetric capacity and low volumetric energy/power density. Therefore, higher solid loading of MWCNTs as active materials is one of the most significant issues to be realized in practice. Very recently, it was argued that nanotube-based active materials have a critical shortcoming in terms of their very low weight per unit electrode area [18]. Thus, their gravimetric energy density may not give a realistic picture to commercial application. The critical limitation may lead to scale-up issues for their potential application in the development of EV. To counter this issue, we propose a new geometry of 3D Cu current collectors, which can play a crucial role in creating higher surface area to accommodate more solid loading of MWCNTs on the uniformly arrayed patterns in the 3D structure, leading to higher specific capacity and C-rate capability. Until now, efforts have been dedicated to employ a number of 3D structured current collectors including carbon papers [19], a self-assembled 3D bicontinuous nanoarchitecture [20], aluminum nanorods [21], and nanoporous nickel [22]. The previous research proved that a self-assembled 3D bicontinuous nanoarchitecture could be one of the ideal electrode architectures in order to realize not only high volume fraction of nanostructured electrolytically active materials (NiOOH/Nickel and MnO_2 cathodes) but also their efficient ion and electron transport [20]. In addition, ALD-coated TiO_2 anodes on 3D aluminum nanorod current collectors showed the 10 times increase in their theoretical area and total capacity (0.0112 $mAhcm^{-2}$), compared to those resulted from the same anodes on 2D flat aluminum plate and high rate capability (the capacity ratios at 10 C/0.5 C and 20 C/0.5 C of the 3D anode were 0.4 and 0.35, respectively.) [21].

Currently, the diverse types of hybrid anode structures have been designed and synthesized in order to expect the synergetic combination of two different types of nanomaterials for the higher electrochemical performances. As one of the most preferable combinations, MWCNTs/Si hybrid structure can be chosen due to the better mechanical accommodation of MWCNTs of the large volume expansion/constriction of Si during lithiation/delithiation process and the higher bonding strength between MWCNTs and Si. There were some selected reports on MWCNTs/Si composite structures, employing either SiH_4 CVD method [23] or sputter deposition [24].

In this study, we present a novel concept 3D anode system, comprising of MWCNTs directly grown on 3D Cu mesh using catalytic thermal CVD method [25]. Electrochemical performances of this 3D anode structure are compared with those of MWCNTs directly grown on 2D Cu foil. Furthermore, enhanced electrochemical properties of a-Si/MWCNTs hybrid structure, synthesized on 3D Cu mesh using a two-step process of CVD and sputtering deposition, are presented. Morphology and structure of as-grown MWCNTs and a-Si/MWCNTs hybrid anode structures and their role in the electrochemical performance are discussed.

2. Experimental

A Cu mesh (TWP Inc.) with average dimensions of 50 μm thickness and 65 μm hole size was prepared. In parallel, a 50 μm thick pure Cu foil (Nimrod Hall Copper, 99.9% purity) was also employed. Both types of samples were used as substrates for depositing Ti (underlayer)/Ni (catalyst) thin film through an RF and DC magnetron sputtering system. These Ti/Ni thin film deposited samples were cut to 14 mm diameter disc shape for 2032 button cell assembly, before being inserted into a thermal CVD system for direct MWCNT growth. During CVD, samples were heated very rapidly, under an inert Ar gas environment, to the growth temperature of 750 °C, and MWCNT growth began with flow of a mixture of ethylene (C_2H_4) and hydrogen (H_2) gases (1:2 volume ratio) in the chamber. After 50 min of growth, the samples were cooled to room temperature within the furnace under an Ar gas envelope. Amorphous Si (a-Si) was further deposited on the as-grown MWCNT samples using the sputtering system with the incorporation of Ti adhesion layer in order to enhance bonding strength between a-Si and MWCNTs. Weights of samples were measured before and after CVD growth to exactly identify weights of the active materials (i.e. MWCNTs and a-Si thin layer).

Morphology and structural properties of the prepared anode structures were carefully investigated using a field emission scanning electron microscope (FESEM) (JEOL, JSM-7000F), an energy dispersive spectroscope (EDS) (Thermo Electron Corporation, NORAN System SIX), a Raman spectrometer (Ar^+ laser with $\lambda = 514$ nm, 33 mW power) and a field emission transmission electron microscope (FETEM) (FEI, TECHNAI F20). Electrochemical performance for these anodic materials was conducted in a typical coin cell (halfcell). The cells were assembled in a CR2032 press. The complete cell assembly was carried out in an argon glovebox under extremely low levels of oxygen and humidity (both individually <0.1 ppm). A pure Li (purity, 99.9%) metal foil (150 μm thickness) was used as both the reference electrode and counter electrodes, while the MWCNTs on 3D Cu mesh, the MWCNTs on 2D Cu foil and the a-Si/MWCNTs composite on 3D Cu mesh were used as the working electrodes. All the coin cells employed a solution 1.0 M $LiPF_6$ in EC-DEC (ethylene carbonate:diethyl carbonate, 1:1 in volume ratio) as the electrolyte and a typical polypropylene–polyethylene material (Celgard 3401) as the separator. The charge–discharge tests of the cells were performed in TOSCAT 3100U multichannel battery testing unit, at a constant temperature of 30 °C, in galvanostatic (constant current density) mode. The cells were cycled in the voltage range 3.0–0.01 V, recording a current value in each 10 mV step, at a slow rate (0.1 C) during the initial formation process and at various C-rates in the following cycles.

3. Results and discussion

3.1. Theoretical calculation of the surface area of 3D Cu mesh

The purpose to introduce 3D Cu mesh as current collector was to increase in surface area for the growth of MWCNTs, thus leading to more amount of Li^+ intake into them, as compared to 2D Cu foil. 3D Cu mesh was an interlaced structure of numerous Cu wires (Appendix A, Fig. 1(a) and (b)). Simple geometrical model was followed to calculate the total surface area of this 3D structure, since the calculation of the actual surface area of the assembled 3D Cu mesh was very difficult. For easier calculation, the cylindrical Cu wires were simplified to rectangular wires of equivalent surface area, creating a cuboid array (Appendix A, Fig. 1(c)). In this study, MWCNTs were synthesized on the top and lateral surface areas of the 3D Cu mesh only, hence only these areas were considered for calculation. Fig. 1(a) was a schematic view of an anode stack built up of 4 layers of MWCNTs on 3D Cu mesh. As a real example, we implemented an anode stack system using 9 individual MWCNTs on 3D Cu mesh, in which MWCNTs were coated over the entire area of the Cu meshes as illustrated in Fig. 1(b). The assembled anodes were physically bonded by adhesion force between the entangled MWCNTs. This phenomenon may be thought of as being in some way analogous to "Velcro" effect of scales on wool fibers [26]. A simple geometrical relationship was established to calculate the total surface area of 3D Cu mesh and 2D Cu foil (no hole). Variation of the surface ratio of 3D Cu mesh to 2D Cu foil as a function of the thickness (T) and the size of holes (L) of 3D Cu mesh is presented in Fig. 1(c) (The detail calculation procedure is shown in the Appendix A.). Surface area increased with the thickness of the structure, though its relation with hole size was not straight forward owing to contribution from a fixed Cu wire diameter. It may be recalled here that the present study used a Cu mesh with its dimension 50 μm thickness and 65 μm hole size, which showed surface area improvement (almost 60%) as compared to 2D Cu foil. Empirically, the average weight of MWCNTs on 3D Cu mesh was 4.37 mg for a cell with 14 mm diameter and 50 μm thickness dimension, which represented solid loading increase by 400%. Thus, it was found that the theoretical calculation was inconsistent with the experimental results since it did not include the influence of control parameters on the properties of MWCNTs such as their diameters, lengths and densities during the CVD growth. From an anode system assembled using 9 individual MWCNTs on 3D Cu mesh (The size of a cell is 15 mm diameter and 50 μm thickness.), the average maximum loading amount and packing density of MWCNTs were higher than 50 mg and 0.248 gcm^{-3}, respectively. The weight of stacked anodes proportionally increased with the number of individual one, which is in a good agreement with the calculation results.

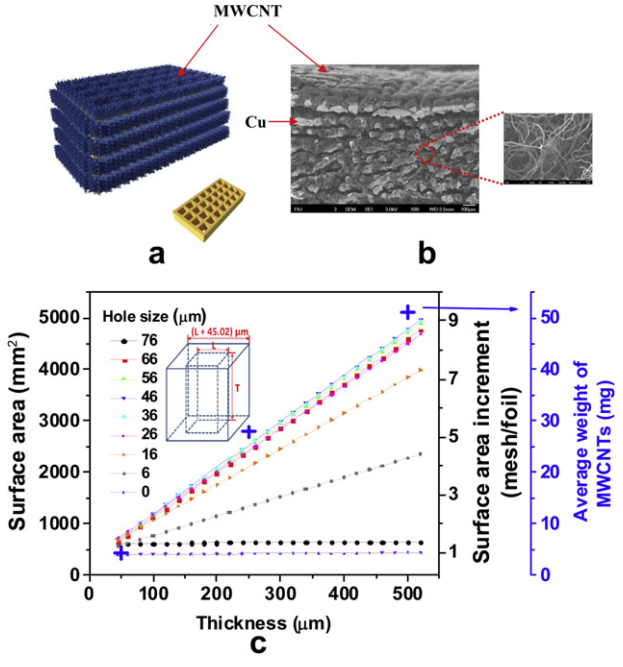

Fig. 1. (a) A schematic model of an anode stack assembled using 4 numbers of converted uniform stacking cuboid arrays from the geometry of a real 3D Cu mesh (The bottom right inset shows a unit cell of the cuboid arrays.), (b) SEM images exhibiting a cross-section perpendicular to the anode system stacked by 9 individual MWCNTs on 3D Cu mesh and highly entangled structures of MWCNTs, (c) The surface area and its increment of the 3D Cu mesh and the 2D Cu foil and the average real weight of MWCNTs as a function of different thickness and hole sizes (The inset illustrates a unit cell of the 3D Cu mesh with its dimension.).

3.2. Morphology and structural properties of MWCNTs and a-Si/MWCNTs on 3D Cu mesh

Unique 3D structure of the proposed anode is expected to influence the electrochemical performance. Structural characterization, involving SEM and Raman spectroscopic analysis, has been conducted on these 3D anodes (see Fig. 2.). As presented in Fig. 2(a), MWCNTs were homogeneously and densely grown over the whole top and lateral Cu mesh area. In addition, the high magnification SEM image showed the randomly entangled MWCNTs with their length around 30 μm and diameter in the range of 200–300 nm (see Fig. 2(b)). Compared to the 2D Cu foil, the surface areas of the Cu wires surrounding the hole spaces could be available sites for the MWCNT growth, which is structural advantage of the 3D Cu mesh to increase the weight of the MWCNTs as active materials. In Fig. 2(c), the sketch of the cross-section view of MWCNTs grown on a single Cu wire exhibited the densely grown larger diameter MWCNTs on the top surface area and relatively smaller diameter MWCNTs on the lateral side area. Along with the structural characteristic, the interfacial control between active materials and current collectors significantly influences the electrochemical performance of the anode system. It is highlighted that the strong bonding between MWCNTs and Cu making it possible to directly grow MWCNTs on Cu mainly stemmed from TiC underlayer [16,27]. The TiC underlayer was formed by the reaction of Ti thin film sputter deposited onto 3D Cu mesh with carbon precursor gas at high temperature about 750°C during CVD processing. High ratio of I_D/I_G (around 1) in Raman spectra (Fig. 2(e)) of the MWCNT structure also revealed high defect density in the structure. It is reported that the MWCNTs containing more defects showed the better electrochemical performance since the higher presence of defects provided with more available sites for Li^+ ion intakes into the MWCNTs structure and shortened the diffusion length of Li^+ ion [28,29]. MWCNTs possessing more defects, generated by mechanical breakage and chemical etching, resulted in an increase in specific capacity compared to untreated MWCNTs. In the case of a-Si/MWCNTs hybrid structure, the broad intensity peak around 480 cm^{-1} (in Raman spectra) showed amorphous Si [30]. It was subsequently confirmed from the EDS analysis in the linearly selected area across the SEM image as shown in Fig. 2(d) that Si was deposited on the some portion of the surface of the MWCNTs. The line profile denoting Si K distinguishably appeared, demonstrating the presence of a-Si deposited layer.

3.3. Electrochemical performances of the MWCNTs based anode systems

3.3.1. Charge/discharge capacities

Electrochemical performance tests were conducted on these anode structures and the results were presented in Fig. 3. First

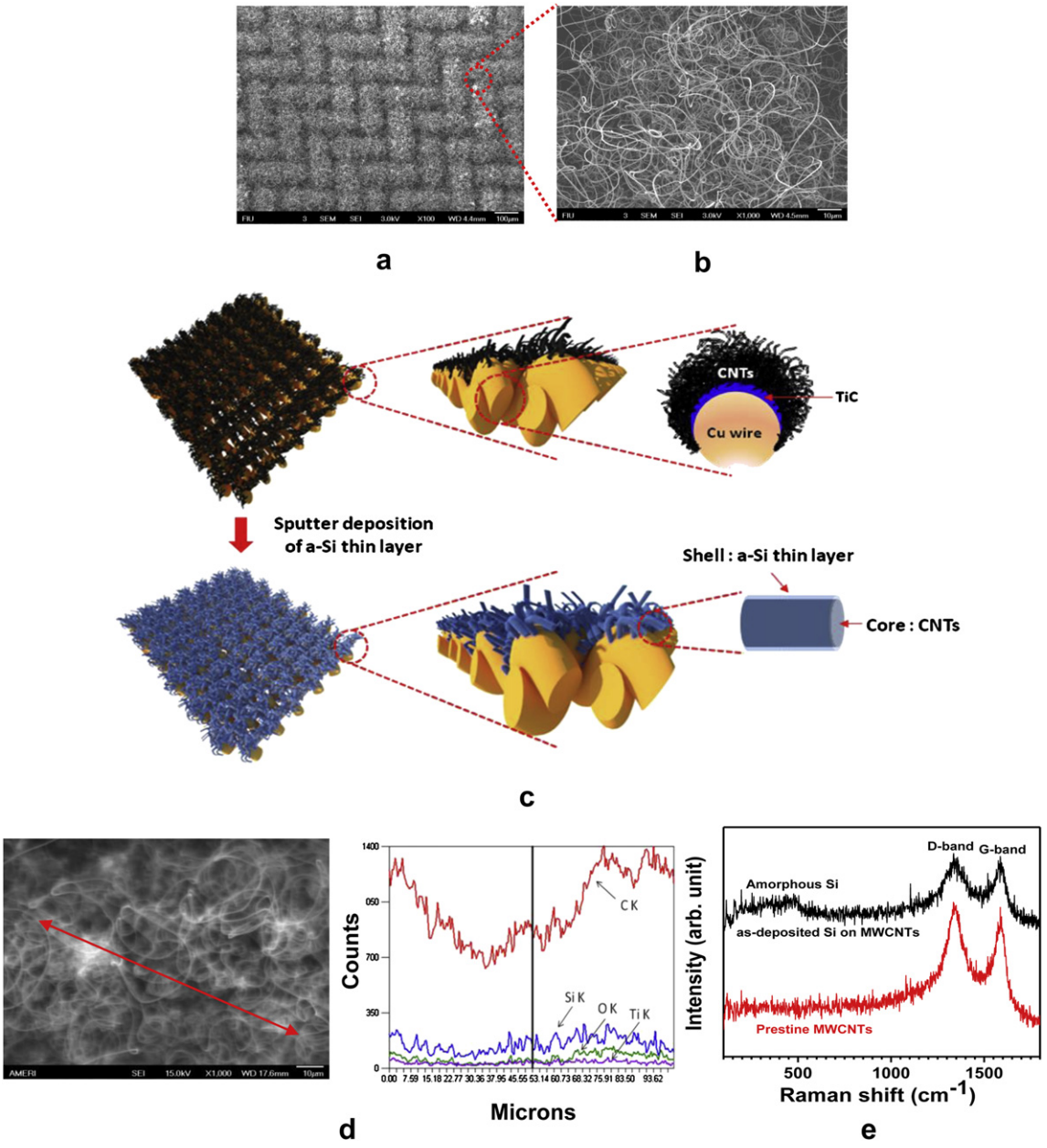

Fig. 2. Morphology and structure of the proposed anode systems. (a) A plane view of SEM image showing the MWCNTs covered on the 3D Cu mesh, (b) The threadlike grass structures of MWCNTs on the 3D Cu mesh with their diameters in the range of 200–300 nm, (c) Schematic diagram (not to scale) of the geometry of the MWCNTs grown on the 3D Cu mesh and the a-Si deposited MWCNTs structure on the 3D Cu mesh, (d) EDS elemental analysis of the a-Si/MWCNTs hybrid structure in the linearly selected area across the SEM image, (e) Raman spectroscopic response indicating high defect density of MWCNTs according to I_D/I_G ratio around 1 and the amorphous Si peak at around 480 cm^{-1} in the a-Si/MWCNTs.

charge–discharge curves for all the anode systems were presented in Fig. 3(a). The button cells were charged/discharged in a galvanostatic mode between 0.01 and 3 V, at C-rate of 0.1 C (specific current 38 mAg^{-1}) determined by theoretical specific capacity of graphite (372 $mAhg^{-1}$). In the case of MWCNTs on 3D Cu mesh electrodes, several samples with different solid loading of MWCNTs were measured under the same condition and showed average discharge capacity 474 $mAhg^{-1}$, $LiC_{4.7}$. In Fig. 3(a), all the discharge curves exhibited a plateau in the voltage range 0.75–0.9 V. Such plateau was found in most graphite or CNT based anodes and stemmed from the decomposition of electrolyte and the formation of solid electrolyte interphase (SEI) on the carbonaceous anode materials [3,31]. Based on the very similar first discharge curves of the MWCNTs and the a-Si/MWCNTs electrodes, it was implied that the MWCNTs mainly controlled the electrochemical properties in the both anode structures since the major weight (above 99% weight ratio) of the structure came from the MWCNTs. However, the effects of a-Si incorporation on the electrochemical performance were investigated by the first charge curves of the both anodes. The average specific charge capacities of the MWCNTs and the a-Si/MWCNTs electrodes were 299 $mAhg^{-1}$ and 345 $mAhg^{-1}$ (almost 16% improvement), respectively. In addition, the Coulombic efficiency of the a-Si/MWCNTs 67% was higher by around 4% than that of the MWCNTs 63%. The relatively higher irreversible capacity at the first charge–discharge cycle is considered a critical limitation of carbonaceous anode materials and the capacity loss may be mainly associated with solid electrolyte interphase (SEI) formation or a permanent alloy formation [31]. Another possible reason

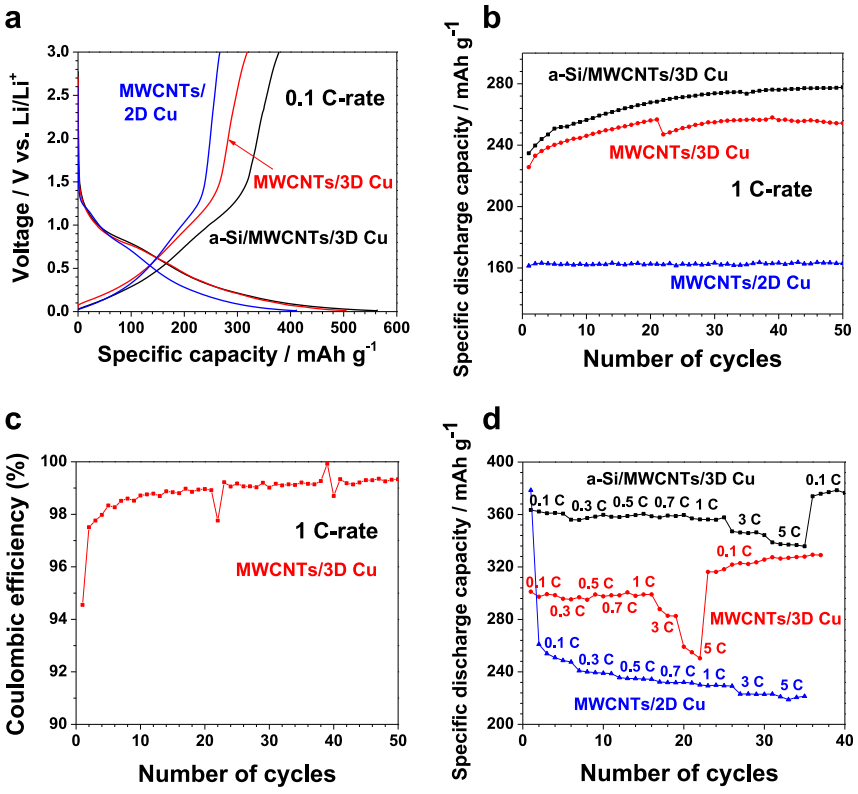

Fig. 3. Electrochemical performance of the anode structures of as-grown MWCNTs on 3D Cu mesh, MWCNTs on 2D Cu foil and a-Si/MWCNTs core–shell composite on 3D Cu mesh. (a) First charge–discharge cycle at 0.1 C-rate, (b) Comparison of the cycling stability of the different anode structures, (c) Coulombic efficiency at 1 C-rate, (d) The variation of reversible capacities at different C-rates.

involved the insertion of lithium ions into defect sites (e.g. micro-cavities) residing in the MWCNTs and their entangled structures [32]. Li ions inserted into the defect regions at the first discharge process might be trapped and could not be completely extracted during the charge process. Lithium oxide formation at higher voltage could also be another reason for the initial capacity loss [33]. However, Fig. 3(a) showed that most Li insertion process proceeded mostly below 1.5 V (versus Li/Li^+) so that the possibility of charge consumption due to lithium oxide formation may be excluded, in the present case. It may be mentioned here that the higher values from the a-Si/MWCNTs indicated the a-Si thin layer could play a role in maintaining the stability of SEI formation [17]. On the contrary, the first discharge curves of all the specimens of the MWCNTs on 2D Cu foil represented the average specific discharge capacity 323 $mAhg^{-1}$, $LiC_{6.9}$. The average capacity value was more than 3 times lower than that of our previous result [16]. It was speculated that the significant difference was due to different morphology of MWCNTs (average diameter 80 nm, which was thinner than that of the current MWCNTs). At higher growth temperature, the size of the catalytic Ni islands became larger on account of their more facile diffusion [34]. With respect to major electrochemically active sites being on and near the surface of MWCNTs [16], the thicker MWCNTs have less active surface area per mass available for participating in electrochemical reaction as compared to the thinner MWCNTs, thereby resulting in the lower specific capacity. During the initial cycle, the MWCNTs on 3D Cu mesh offered 47% higher average specific capacity compared to that of the MWCNTs on 2D Cu foil. It may be noted here that this specific capacity enhancement is close to surface area enhancement 60% also. Compared to the MWCNTs on 3D Cu anodes, the a-Si deposited MWCNT anodes offered the higher average specific discharge capacity 517 $mAhg^{-1}$, $LiC_{4.3}$. This enhancement could be related to the presence of a-Si thin layer with its high specific capacity on the MWCNTs. It was observed that the weight of the deposited a-Si was lower than 1% of that of the MWCNTs; therefore, the a-Si thin layer did not have any major contribution except slight increase in the overall specific capacity of the anode, unlike the previous results from Si nanotubes [6] and Si nanowires [7].

3.3.2. *Cycling stability*

Cycling stability tests are essential to prove electrochemical performance of the anodes at long cycling operation in the real application. Fig. 3(b) illustrates a comparison of the cycling stabilities obtained from the three different kinds of anode systems up to 50 cycles at 1 C-rate (current density 372 mAg^{-1}). In the case of the MWCNTs on 3D Cu mesh electrode, the reversible capacity slightly increased from 226 $mAhg^{-1}$ at first cycle to 258 $mAhg^{-1}$ at 39th cycle and then gradually faded to 254 $mAhg^{-1}$ until 50th cycles. Such a trend of increase in capacity over the whole cycles is inconsistent with previous results from the constant capacity of MWCNT [16,17]. It was speculated that the continuous charge–discharge process led to create more surface area on the densely entangled MWCNT network structure. We also investigated whether such an activation process was due to more defects in the structures of MWCNTs induced by the charge–discharge process. According to the SEM images presented in Fig. 4(a) and (b), it was not evident that severe defects or structural damages appeared in the both 150 cycled and just one discharged anode systems. HRTEM images revealed that for both the anode systems, the structural integrity of graphene layers still remained with the shallow amorphous second phase region on the edge of the MWCNTs as shown in Fig. 4(c) and (d). In addition, it was pointed out that there was no appreciable volume variation during lithiation and delithiation. No clear evidence of diameter change was

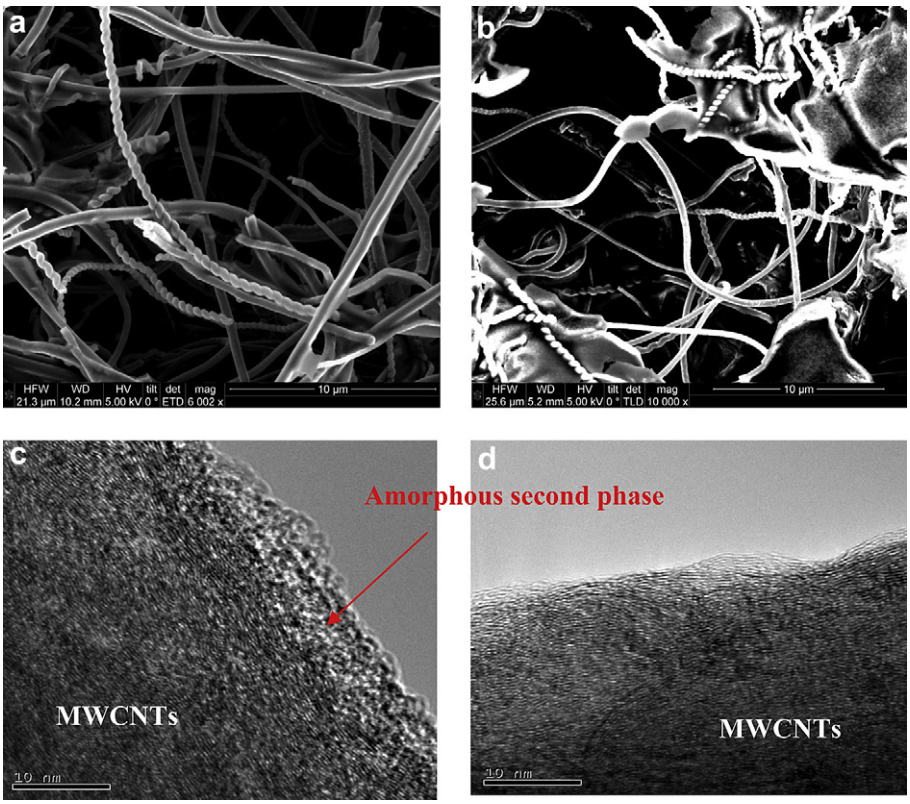

Fig. 4. Plane view SEM images of (a) the MWCNTs on 3D Cu mesh anodes after 150 cycling at 1 C-rate and (b) the MWCNTs after only 1 discharge cycling at the same C-rate. HRTEM images of (c) the 150 cycled one and (d) the 1 discharge cycled one.

observed between the as-grown MWCNTs and the MWCNTs subjected to 150 charge–discharge cycles (Figs. 2(b) and 4(a)). This observation is in agreement with small volume change of graphitic carbon upon lithium insertion and extraction (typically LiC_6, around 12%) [35]. In the same manner, it was confirmed that the specific capacity of the a-Si/MWCNTs on 3D Cu was gradually increased.

Along with the electrochemical activation process of MWCNTs, the result could reveal the effect of capacity improvement with additionally incorporated a-Si to take more Li^+ ion intakes (almost 10% enhancement of the reversible capacity). Furthermore, the Si–C bonding at the interface between a-Si and MWCNTs was strong enough to avoid peeling off of the a-Si layer during the cycling test. It was highlighted that MWCNTs and a-Si/MWCNTs grown on 3D Cu mesh showed good cycling stability without severe capacity degradation. However, for the MWCNTs on 2D Cu foil, the average reversible capacity 163 $mAhg^{-1}$ was kept constant until the number of 50 cycles. It should be noted that the larger reversible capacity of the 3D MWCNTs was presumably due to their large surface area to accommodate more Li^+ ion intercalation. In terms of the reversibility of charge–discharge process, the Coulombic efficiency of the MWCNTs on 3D Cu mesh was more than 98% after the initial 4 cycles at 1.0 C-rate and then increased to 99% after 22 cycles according to the result shown in Fig. 3(c). Such reversibility was ascribed to the sufficient supply of Li^+ ions from Li metal foil used as the reference electrode and counter electrode in the button cell.

3.3.3. Rate capability

Rate capability tests are also crucial to prove electrochemical performance of the anodes at higher charge–discharge rate operation. Fig. 3(d) showed the rate capability of the proposed anodes. The discharge capacity of the MWCNTs on 3D Cu mesh was almost constant around 300 $mAhg^{-1}$ until reaching 1 C-rate (372 mAg^{-1}) and then decreased to 283 $mAhg^{-1}$ at 3 C-rate (1116 mAg^{-1}) and further to 250 $mAhg^{-1}$ at 5 C-rate (1860 mAg^{-1}). It may be highlighted that discharge capacity slightly increased with C-rate from 0.1 C to 1 C and the phenomenon could be attributed to the electrochemical activation process of MWCNTs during cycling as mentioned above. At higher C-rates (e.g. 3 C and 5 C), Li^+ ions were inserted and extracted into and from the only surface regions of the forest-like MWCNTs structure due to the limitation of diffusion length of Li^+ ions. Another interesting observation was slight increase in specific capacity from 283 $mAhg^{-1}$ at 1st cycle to 320 $mAhg^{-1}$ at 22nd cycle at the same 0.1 C rate (38 mAh g^{-1}). It was again confirmed that higher number of cycles during C-rate tests could be a reason to effectively carry out electrochemical activation process in the MWCNT structures. On the contrary, the MWCNTs on 2D Cu foil electrode showed a typical staircase type decreasing capacity behavior till the tested limit of 5 C-rate. The direct comparison revealed the higher C-rate capability of the MWCNTs on 3D Cu mesh electrode, as compared to the MWCNTs on 2D Cu foil. In particular, at 5 C, the average specific discharge capacity of the MWCNTs on 3D Cu mesh was 249 $mAhg^{-1}$ (14% increase), whereas that of the MWCNTs on 2D Cu foil was 218 $mAhg^{-1}$. The result could be strongly associated with the higher surface area for Li^+ ion intercalation due to approximately 4 times higher solid loading of MWCNTs on 3D Cu mesh. Furthermore, the higher C-rate capability is significantly attributed to the strong bonding and the lower electric resistance between Cu and MWCNTs, through TiC interface layer [36,37]. Moreover, at 5 C, the average capacity of the a-Si/MWCNTs on 3D Cu mesh electrode was 334 $mAhg^{-1}$ (34% enhancement), while that of the MWCNTs on 3D Cu mesh was 249 $mAhg^{-1}$. In addition, the average capacity ratios at 5 C/0.1 C of the MWCNTs on 3D Cu mesh and the MWCNTs on 2D Cu foil were

0.86 and 0.8, respectively, whereas the ratio of the a-Si/MWCNTs on 3D Cu mesh was around 0.93. According to the better performances, it was proved that a-Si thin layer coating on MWCNTs could play an important role in the enhancement of C-rate capability.

4. Conclusion

A novel 3D MWCNTs on Cu current collectors as an anode of LIB was developed. The 3D anodes showed higher specific capacity, cycling stability and C-rate efficiency as compared to those of the MWCNTs on 2D Cu foil anodes. The better performances of the 3D anodes were attributed to the higher average solid loading of MWCNTs, which was 4 times higher than that of the 2D anodes. Addition of the a-Si onto the 3D MWCNTs/Cu showed the further enhancement of electrochemical properties.

Acknowledgment

Authors thank N. Ricks and Y. Liu for Nano fabrication facility and FESEM characterization, S. Saxena for allowing to use the Raman facility and J. Hwang and R. Banerjee for HRTEM characterization. It is grateful that J. Kim and D. Kim who provided us with the schematic diagrams. This research was, in part, supported by WCU (World Class University) program through the Korea Science and Engineering Foundation funded by the Ministry of Education, Science and Technology (R31-2008-000-10092) and AFOSR Grant (FA9550-09-1-0544).

Appendix A. Supplementary material

Supplementary material associated with this article can be found, in the online version, at http://dx.doi.org/10.1016/j.jpowsour.2012.07.050.

References

[1] T. Nagaura, K. Tozawa, Prog. Batteries Sol. Cells 9 (1990) 209.
[2] L.F. Nazar, O. Crosnier, in: G.-A. Nazri, G. Pistoia (Eds.), Lithium Batteries: Science and Technology, Springer, New York, 2004, pp. 112–115.
[3] M. Winter, K.-C. Moeller, J.O. Besenhard, in: G.-A. Nazri, G. Pistoia (Eds.), Lithium Batteries: Science and Technology, Springer, New York, 2004, pp. 144–194.
[4] R.A. Huggins, Advanced Batteries Materials Sciences Aspects, Springer, New York, 2010.
[5] D. Larcher, S. Beattie, M. Morcrette, K. Edstroem, J.C. Jumas, J.M. Tarascon, J. Mater. Chem. 17 (2007) 3759–3772.
[6] M.H. Park, M.G. Kim, J.B. Joo, K.T. Kim, J.Y. Kim, S.H. Ahn, Y. Cui, J.P. Cho, Nano Lett. 9 (2009) 3844–3847.
[7] C.K. Chan, H.L. Peng, G. Liu, K. McIlwrath, X.F. Zhang, R.A. Huggins, Y. Cui, Nat. Nanotechnol. 3 (2008) 31–35.
[8] P. Poizot, S. Laruelle, S. Grugeon, L. Dupont, J.M. Tarascon, Nature 407 (2000) 496–499.
[9] E. Hosono, S. Fujihara, I. Honma, H. Zhou, Electrochem. Commun. 8 (2006) 284–288.
[10] B. Varghese, M.V. Reddy, Z. Yanwu, C.S. Lit, T.C. Hoong, G.V.S. Rao, B.V.R. Chowdari, A.T.S. Wee, C.T. Lim, C.-H. Sow, Chem. Mater. 20 (2008) 3360–3367.
[11] E.J. Yoo, J. Kim, E. Hosono, H.-S. Zhoi, T. Kudo, I. Honma, Nano Lett. 8 (2008) 2277–2282.
[12] G. Che, B.B. Lakshmi, E.R. Fisher, C.R. Martin, Nature 393 (1998) 346–349.
[13] A.L.M. Reddy, M.M. Shaijumon, S.R. Gowda, P.M. Ajayan, Nano Lett. 9 (2009) 1002–1006.
[14] A. Varzi, C. Täubert, M. Wohlfahrt-Mehrens, M. Kreis, W. Schütz, J. Power Sources 196 (2011) 3303–3309.
[15] B.J. Landi, M.J. Ganter, C.D. Cress, R.A. DiLeo, R.P. Raffaelle, Energy Environ. Sci. 2 (2009) 638–654.
[16] I. Lahiri, S.W. Oh, J.Y. Hwang, S.J. Cho, Y.K. Sun, R. Banerjee, W.B. Choi, ACS Nano 4 (2010) 3440–3446.
[17] I. Lahiri, S.M. Oh, J.Y. Hwang, C.W. Kang, M.S. Choi, H.T. Jeon, R. Banerjee, Y.K. Sun, W.B. Choi, J. Mater. Chem. 21 (2011) 13621–13626.
[18] Y. Gogotsi, P. Simon, Science 34 (2011) 917–918.
[19] C. Arbizzani, S. Beninati, M. Lazzari, M. Mastragostino, J. Power Sources 141 (2005) 149–155.
[20] H. Zhang, X. Yu, P.V. Braun, Nat. Nanotechnol. 6 (2011) 277–281.
[21] S.K. Cheah, E. Perre, M. Rooth, M. Fondell, A. Hårsta, L. Nyholm, M. Boman, T. Gustafsson, J. Lu, P. Simon, K. Edström, Nano Lett. 9 (2009) 3230–3233.
[22] Y.Q. Zhang, X.H. Xia, X.L. Wang, Y.J. Mai, S.J. Shi, Y.Y. Tang, C.G. Gu, J.P. Tu, J. Power Sources 213 (2012) 106–111.
[23] L.F. Cui, Y. Yang, C.M. Hsu, Y. Cui, Nano Lett. 9 (2009) 3370–3374.
[24] P.-C. Chen, J. Xu, H. Chen, C. Zhou, Nano Res. 4 (2011) 290–296.
[25] W. Choi, I. Lahiri, C. Kang, United States Provisional Patent 61,567,979.
[26] S.V. Lomov, L. Gorbatikh, I. Verpoest, Carbon 49 (2011) 2079–2091.
[27] I. Lahiri, R. Seelaboyina, J.Y. Hwang, R. Banerjee, W. Choi, Carbon 48 (2010) 1531–1538.
[28] B. Gao, C. Bower, J.D. Lorentzen, L. Fleming, A. Kleinhammes, X.P. Tang, L.E. McNeil, Y. Wu, O. Zhou, Chem. Phys. Lett. 327 (2000) 69–75.
[29] H.-C. Shin, M. Liu, B. Sadanadan, A.M. Rao, J. Solid State Electrochem. 8 (2004) 908–913.
[30] Z. Iqbal, S. Vepiek, J. Phys. C: Solid State Phys. 15 (1982) 377–392.
[31] C.D.L. Casas, W. Li, J. Power Sources 208 (2012) 74–85.
[32] G. Wang, X. Shen, J. Yao, D. Wexler, J.H. Ahn, Electrochem. Commun. 11 (2009) 546–549.
[33] E. Frackowiak, S. Gautier, H. Gaucher, S. Bonnamy, F. Beguin, Carbon 37 (1999) 61–69.
[34] Y.T. Lee, J. Park, Y.S. Choi, H. Ryu, H.J. Lee, J. Phys. Chem. B 106 (2002) 7614–7618.
[35] S. Bhattacharya, A.R. Riahi, A.T. Alpas, J. Power Sources 196 (2011) 8719–8727.
[36] I. Lahiri, W.B. Choi, Acta Mater. 59 (2011) 5411–5421.
[37] I. Lahiri, D. Lahiri, S. Jin, A. Agarwal, W.B. Choi, ACS Nano 5 (2011) 780–787.